Negative-to-Positive Tunnel Magnetoresistance in van der Waals $Fe_3GeTe_2/Cr_2Ge_2Te_6/Fe_3GeTe_2$ Junctions

Zi-Ao Wang(王子奥)[1,2], Xiaomin Zhang(张晓敏)[1,2], Wenkai Zhu(朱文凯)[1], Faguang Yan(闫法光)[1], Pengfei Liu(刘鹏飞)[1], Zhe Yuan(袁喆)[3], and Kaiyou Wang(王开友)[1,2*]

[1]*State Key Laboratory of Superlattices and Microstructures, Institute of Semiconductors, Chinese Academy of Sciences, Beijing 100083, China*
[2]*Center of Materials Science and Optoelectronics Engineering, University of Chinese Academy of Sciences, Beijing 100049, China*
[3]*Center for Advanced Quantum Studies and Department of Physics, Beijing Normal University, Beijing 100875, China*

(Received 13 April 2023; accepted manuscript online 2 June 2023)

The emergent van der Waals magnetic material is a promising component for spintronic devices with novel functionalities. Here, we report a transition of negative-to-positive magnetoresistance in $Fe_3GeTe_2/Cr_2Ge_2Te_6/Fe_3GeTe_2$ van der Waals all-magnetic tunnel junctions with increasing the applied bias voltage. A negative magnetoresistance is observed first in $Fe_3GeTe_2/Cr_2Ge_2Te_6/Fe_3GeTe_2$ tunnel junctions, where the resistance with antiparallel aligned magnetization of two Fe_3GeTe_2 electrodes is lower than that with parallel alignment, which is due to the opposite spin polarizations of two Fe_3GeTe_2 electrodes. With the bias voltage increasing, the spin polarization of the biased Fe_3GeTe_2 electrode is changed so that the spin orientations of two Fe_3GeTe_2 electrodes are the same. Our experimental observations are supported by the calculated spin-dependent density of states for Fe_3GeTe_2 electrodes under a finite bias. The significantly bias voltage-dependent spin transport properties in van der Waals magnetic tunnel junctions open a promising route for designing electrical controllable spintronic devices based on van der Waals magnets.

DOI: 10.1088/0256-307X/40/7/077201

Magnetic tunnel junction (MTJ) is a fundamental structure of great significance in spintronics,[1–4] whose basic structure consists of two ferromagnetic metals inserted by an insulating interlayer as a tunnel barrier. High-quality interfaces play a key role in the process of spin-polarized electrons tunneling through the junction.[5,6] The recently emerged van der Waals magnets with atomically sharp interfaces[7–10] offer the appropriate scenario to study the tunnel magnetoresistance effect.[11–14] Up to date, a variety of van der Waals magnets have been discovered, including ferromagnetic metals,[15,16] ferromagnetic semiconductors,[17,18] ferromagnetic topological insulators,[19] antiferromagnetic semiconductors,[20] and antiferromagnetic topological insulators.[21] Among them, Fe_3GeTe_2 (FGT) is one of the most concerned and extensively studied van der Waals ferromagnetic metals, which exhibits a relatively high Curie temperature $T_C \sim 220$ K and strong perpendicular magnetic anisotropy.[22,23] This makes FGT an excellent candidate for the ferromagnetic electrode in spin-valve devices.[24–26] Various van der Waals interlayers sandwiched by FGT electrodes such as FGT/hBN/FGT,[27,28] FGT/graphite/FGT,[29] FGT/MoS_2/FGT,[30] and FGT/InSe/FGT[31] have been investigated experimentally to date.

The coercive fields H_c of the top or bottom Fe_3GeTe_2 electrode in $Fe_3GeTe_2/Cr_2Ge_2Te_6/Fe_3GeTe_2$ van der Waals all-magnetic tunnel junction can be selectively controlled by applied directional electric fields.[32] In this MTJ, the interlayer $Cr_2Ge_2Te_6$ (CGT) is a van der Waals ferromagnetic semiconductor with perpendicular magnetic anisotropy and a small coercivity of ~ 3.4 mT below 65 K (T_C of bulk CGT).[33] A negative magnetoresistance effect is observed in FGT/CGT/FGT MTJ with bias voltage below 0.80 V, which originates from the opposite spin polarization of two FGT electrodes.[32,34] However, under a higher bias, the spin polarization of FGT may be reversed due to the excited high-energy localized spin states,[28] which will lead to the changed sign of magnetoresistance and still has not been investigated in FGT/CGT/FGT MTJ experimentally.

In this Letter, we demonstrate the changed sign of tunneling magnetoresistance in FGT/CGT/FGT MTJs with the applied bias voltage raising. A negative magnetoresistance is observed in FGT/CGT/FGT MTJs with bias voltage ranging from 0.40 V to 0.90 V and transformed to a positive one above 0.90 V. The magnetoresistance signal is undetectable below 0.40 V. Based on first-principles calculations, this transition of magnetoresistance effect originates from the inversion of spin polarization of the biased FGT electrode.

We fabricated five FGT/CGT/FGT MTJs using mechanical exfoliation of CGT and FGT crystals (HQ Graphene company) and dry transfer technique (see Methods in the Supplementary Information for details). The CGT interlayer is sandwiched by two FGT electrodes (top-FGT electrode is thicker than bottom-FGT electrode, guaranteeing different coercive fields) in all these 5 devices and only the thicknesses of the CGT interlayers are differ-

*Corresponding author. Email: kywang@semi.ac.cn
© 2023 Chinese Physical Society and IOP Publishing Ltd

ent. From device 1 to device 5, the thicknesses of CGT interlayers are increasing from 4 nm to 9 nm. The junction areas of these FGT/CGT/FGT MTJs are approximately 2–5 μm^2. To prevent oxidation, all these samples are prepared in a nitrogen-filled glove box and measured in a cryogenic probe station with an ultra-high vacuum environment. The electrical and magneto-transport properties of FGT/CGT/FGT MTJs were measured by the two-terminal method, as shown in Fig. 1(a). For eliminating the resistance change caused by different junction areas in these devices, we show the curves of current density versus voltage (J–V) instead of current–voltage (I–V) curves for them in Fig. 1(b), which are measured at 10 K. All of the J–V curves exhibit nonlinear behavior, confirming the tunneling characteristic of these devices. Because of the thicker interlayer and then the larger junction resistance,[35] the applied voltage to the devices would be higher so as to reach the same current density. The calculated resistance-area product ($R{\cdot}A$) of each device at the same current density of 0.5 $A{\cdot}cm^{-2}$ is shown in Fig. 1(c).

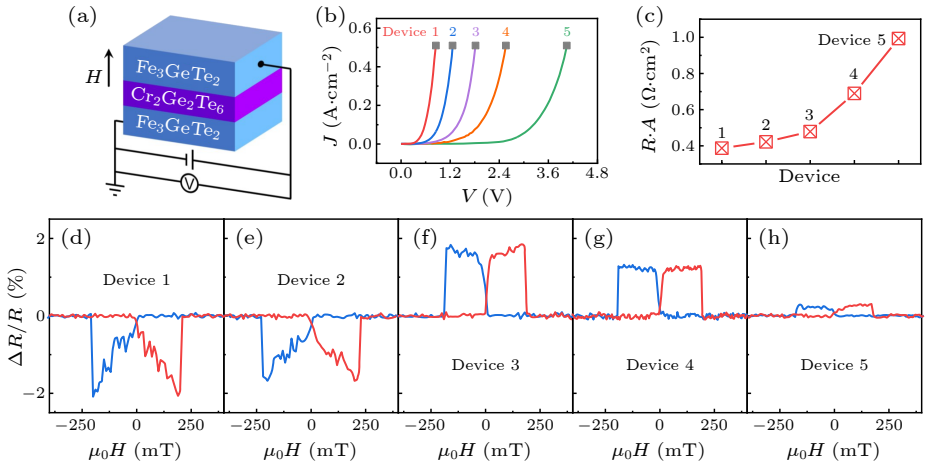

Fig. 1. Device configuration, electrical and magneto-transport properties. (a) Schematic of the FGT/CGT/FGT MTJ. (b) Nonlinear curves of current density versus voltage (J–V) for devices 1, 2, 3, 4, and 5, measured at 10 K. (c) Resistance-area product ($R \cdot A$) of each device calculated numerically at the same current density of 0.5 $A{\cdot}cm^{-2}$, as shown by the grey squares in (b). (d)–(h) Magnetoresistance curves of devices 1, 2, 3, 4, and 5, measured with $J_{bias} = 50\,mA{\cdot}cm^{-2}$ at 10 K.

We then measured the resistance (R) of these devices by scanning the external perpendicular magnetic field (H) under the same bias current density ($J_{bias} = 50\,mA{\cdot}cm^{-2}$) at 10 K. During the measurement, the magnetic field is scanned from a sufficiently large $H \sim -500$ mT to ensure the parallel magnetization alignment of two FGT electrodes at the beginning. We define the magnetoresistance as $\Delta R/R = (R_{AP} - R_P)/R_P$, where R_{AP} and R_P are the resistances with antiparallel and parallel magnetization alignments of the ferromagnetic electrodes, respectively. The measured magnetoresistance hysteresis loops ($\Delta R/R$–H) are plotted in Figs. 1(d)–1(h), where a transition from the negative ($\Delta R/R < 0$, devices 1 and 2) to the positive ($\Delta R/R > 0$, devices 3, 4 and 5) magnetoresistance can be observed. For devices 1 and 2, the high- and low-resistance states represent the resistance with parallel (↑↑ or ↓↓) and antiparallel (↑↓ or ↓↑) aligned magnetizations of two FGT electrodes (see Fig. S1(a) in the Supplementary Information), respectively, which has been reported in the work about FGT/CGT/FGT MTJs.[32] For devices 3, 4, and 5, the relationship between the magnetization alignments and the resistance states is reversed: the high-resistance state represents the resistance with antiparallel (↑↓ or ↓↑) aligned magnetization while the low state represents the parallel (↑↑ or ↓↓) alignment (see Fig. S1(b) in the Supplementary Information). Considering that the junction resistance increases from device 1 to device 5, under the same bias current density, the equivalent bias voltage during the magnetoresistance measurements becomes higher sequentially. Therefore, we speculate that the higher bias voltage is the reason for positive magnetoresistance in devices 3, 4, and 5. To verify this, we chose device 2 for further magneto-transport measurements.

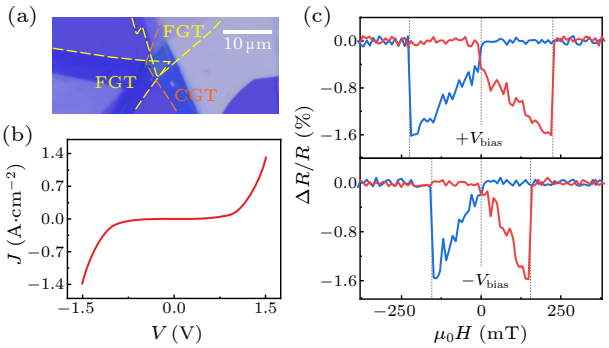

Fig. 2. Magneto-transport measurements of the FGT/CGT/FGT MTJ under opposite biases. (a) The optical image of a typical FGT/CGT/FGT MTJ (device 2), where the edges of FGT electrodes and CGT interlayer are outlined in yellow and orange, respectively. (b) The J–V curve for device 2 at 10 K. (c) The magnetoresistance curves for device 2 with $+V_{bias} = 0.75$ V (upper) and $-V_{bias} = -0.75$ V (lower), measured at 10 K. The grey dotted lines indicate the positions of switching fields.

Figure 2(a) shows the optical image of the FGT/CGT/FGT MTJ (i.e., device 2), where the FGT electrodes are outlined in yellow and the CGT interlayer is outlined in orange. The thickness of CGT interlayer

in device 2 is confirmed by atomic force microscopy of ~ 4.8 nm (see Fig. S2 in the Supplementary Information). The nonlinear behavior is exhibited under both positive and negative voltages, as shown in Fig. 2(b). It is noticed that in the magnetoresistance curves of these five devices [Figs. 1(d)–1(h)], there is always a resistance switching field ~ 0 mT, which is due to the lowered electron density and dramatically reduced magnetic anisotropy energy of one FGT electrode, caused by electric field-enhanced directional charge transfer from FGT to CGT at the CGT/FGT interface.[32] The manipulated FGT electrode can be selected by changing the direction of the external applied electric field, therefore the switching fields of the FGT/CGT/FGT MTJ under opposite biases are different, as shown in Fig. 2(c). In these magnetoresistance curves, the switching fields are ~ 0 mT/220 mT under positive bias voltage $V_{\rm bias} = 0.75$ V, and ~ 0 mT/150 mT under negative bias voltage $-V_{\rm bias} = -0.75$ V. The obviously different switching fields of ~ 220 mT and ~ 150 mT are attributed to the initial coercivity of top- and bottom-FGT electrodes, respectively.

Furthermore, we investigated the bias voltage-dependent magneto-transport properties of the FGT/CGT/FGT MTJ. Figures 3(a)–3(f) present the magnetoresistance curves of device 2 under different $V_{\rm bias}$ ranging from 0.75 V to 1.50 V. A transition from negative to positive is observed above 0.90 V. In addition, the tunneling process of electrons in the FGT/CGT/FGT MTJ with $V_{\rm bias}$ below 0.40 V is undetectable due to the noise of experimental environment and the high tunnel barrier in this device. The measured negative magnetoresistance with $V_{\rm bias}$ between 0.40 V and 0.75 V can be seen in our previous work.[32] It is noted that, as the bias voltage raises, the magnetoresistance curves vary from a 'triangle' to a 'stage' shape. When the bias voltage is low ($V_{\rm bias} \leq 0.90$ V, the electric field pointing toward the bottom FGT electrode), the enhanced charge transfer at bottom CGT/FGT interface results in a negligible perpendicular or even an in-plane anisotropy field in the bottom FGT electrode, which leads to the magnetoresistance curves exhibiting the triangle behavior. Under a higher bias ($V_{\rm bias} > 0.90$ V), the electron flow through the junction becomes larger as well as the spin-transfer torque becomes stronger, which helps to switch the bottom FGT electrode to keep it perpendicular, leading to the stage behavior in the magnetoresistance curves.[32,36]

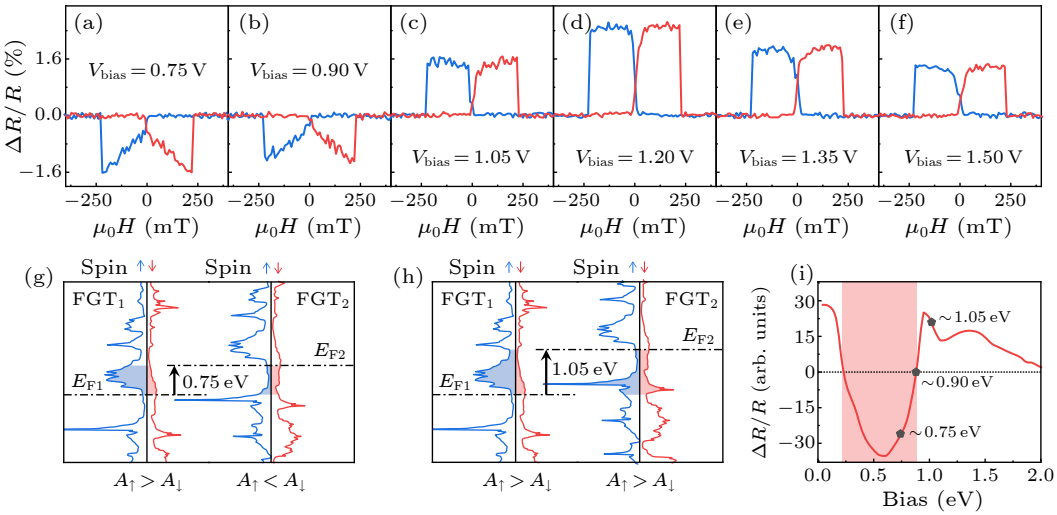

Fig. 3. Negative and positive magnetoresistances of the FGT/CGT/FGT MTJ. (a)–(f) The magnetoresistance curves for device 2 with different $V_{\rm bias}$ ranging from 0.75 V to 1.50 V, measured at 10 K. [(g), (h)] Calculated spin-dependent DOS for FGT electrodes, where FGT_1 is always grounded and FGT_2 is biased at 0.75 eV and 1.05 eV with respect to FGT_1. The blue and red shaded regions show portions of DOS with spin-up ↑ and spin-down ↓ that take part in the tunneling process, whose areas are marked as $A_\uparrow$ and $A_\downarrow$. (i) The resultant magnetoresistance versus bias curve numerical calculated from DOS. The red shaded region represents the negative magnetoresistance.

In order to illustrate the mechanism of the magnetoresistance sign change above 0.90 V, we study the spin-dependent density of state (DOS) of FGT electrodes performed by first-principles calculations, under the finite bias of 0.75 eV and 1.05 eV in Figs. 3(g) and 3(h), respectively. In this model, the bottom-FGT (FGT_1) is always grounded to maintain a constant Fermi energy and the bias is applied to the top-FGT (FGT_2). The blue and red shaded regions in Figs. 3(g) and 3(h) represent the spin-up ↑ and spin-down ↓ states lying between the two Fermi levels ($E_{\rm F1}$ and $E_{\rm F2}$), respectively, which contribute to the tunneling current. The areas of them ($A_\uparrow$ and $A_\downarrow$) can be obtained by numerical integration of spin ↑ and spin ↓ states, respectively. When the bias is 0.75 eV [Fig. 3(g)], the spin polarizations of FGT_1 and FGT_2 are opposite ($A_\uparrow > A_\downarrow$ for FGT_1 and $A_\uparrow < A_\downarrow$ for FGT_2), resulting in a negative magnetoresistance.[34] When the bias increases to 1.05 eV, the portions of DOS with up-spin ↑ and down-spin ↓ that take part in the tunneling process are changed, as shown in Fig. 3(h). In this case, as $A_\uparrow > A_\downarrow$ for both FGT_1 and FGT_2, FGT_1 and FGT_2 have the same spin orientation and result in the positive magnetoresistance. The full magnetoresistance versus bias curve numerically calculated from DOS is shown in Fig. 3(i), where the sign change occurs at ~ 0.90 eV, which shows only a minor deviation from the experimental observations (between 0.90 V

and 1.05 V). In addition, in the FGT/CGT/FGT MTJ, the electrons directly tunneled through the CGT layer without electron accumulation, which is different from the gate voltage control. Therefore, there is no noticeable modulation of the density of states in CGT by the bias voltage.

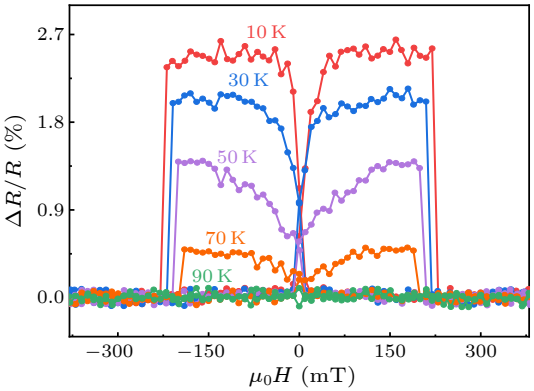

Fig. 4. Temperature dependence of magneto-transport properties of the FGT/CGT/FGT MTJ. The magnetoresistance curves for device 2 with $V_{\rm bias} = 1.20$ V at different temperatures ranging from 10 K to 90 K.

Comparing the magnitude of positive magnetoresistance under different $V_{\rm bias}$, we note that $\Delta R/R$ increases with raising $V_{\rm bias}$ to 1.20 V, and then begins to decrease. The highest $\Delta R/R$ at $V_{\rm bias} = 1.20$ V can be attributed to the electrons gaining energy to overcome the tunnel barrier completely, while the electrons under higher $V_{\rm bias}$ with more energy have a larger probability of scattering by local ions and trapping states at the interfaces.[37] We then performed the magneto-transport measurements under different temperatures with the same $V_{\rm bias}$ (1.20 V), as shown in Fig. 4, where the magnetoresistance decreases monotonically with increasing temperature. According to the previous reports about spin-valve devices with FGT electrodes, the magnetoresistance signal always vanishes at $T_{\rm C} \sim 220$ K of FGT,[24] however we note that $\Delta R/R$ of the FGT/CGT/FGT MTJ becomes zero at ~ 90 K. Due to the enhanced charge transfer from FGT to CGT by electric fields, the interfacial layer of CGT is metalized with partially occupied conduction bands, revealed by calculating the layer-resolved DOS,[32] which makes the effective barrier width thinner than the actual thickness of CGT interlayer. When the temperature is above $T_{\rm C} \sim 65$ K of CGT, the ferromagnetic CGT transforms into paramagnetic CGT, which may lead to the number of transfer electrons different. The weakened metallization of the interfacial CGT layer around $T_{\rm C}$ of CGT is also confirmed by temperature-dependent J–V curves for device 2 (see Fig. S3 in the Supplementary Information). Meanwhile, as the temperature increases, the magnetization of the ferromagnetic FGT decreases, following the Bloch's law due to the stronger thermal fluctuations. Since the spin polarization of FGT electrodes is proportional to the magnetization, the spin polarization decreases with increasing temperature.[27] The combination of these two effects makes $\Delta R/R$ of the FGT/CGT/FGT MTJ decrease rapidly as the temperature raises.

The FGT/CGT/FGT MTJ in our work is essentially different from the FGT/FGT/FGT spin valve reported in the literature.[24] Compared with the all-metallic FGT/FGT/FGT spin valve with linear current-voltage curves, the electron transport processes are different in the FGT/CGT/FGT MTJ, which exhibits a tunneling characteristic with nonlinear behavior. Due to the low resistance and low voltage across the FGT/FGT/FGT spin valve, the spin polarization reversal of FGT under a higher bias and the resultant phenomena, including the negative magnetoresistance effect as well as the sign change of magnetoresistance effect, are not observed in the FGT/FGT/FGT spin valve. Furthermore, the selectively controlled FGT electrodes originated from the directional charge transfer from FGT to CGT are also not observed in the FGT/FGT/FGT spin valve.

In summary, we have demonstrated a sign change of magnetoresistance in FGT/CGT/FGT MTJs. With the bias voltage increasing, the magnetoresistance changes from negative to positive. We attribute this transition to the inverted spin polarizations of the biased FGT electrode, which leads to the opposite spin orientations of two FGT electrodes becoming the same. Our work provides a comprehensive insight into FGT/CGT/FGT magnetic tunnel junction devices, which promotes the development of novel spintronic devices based on van der Waals magnetic materials.

Acknowledgments. This work was supported by the National Key Research and Development Program of China (Grant No. 2022YFA1405100), the Beijing Natural Science Foundation Key Program (Grant No. Z190007), the Strategic Priority Research Program of Chinese Academy of Sciences (Grant Nos. XDB44000000 and XDB28000000), and the National Natural Science Foundation of China (Grant Nos. 12241405, 11734004, and 12174028).

References

[1] Žutić I, Fabian J, and Sarma S D 2004 *Rev. Mod. Phys.* **76** 323
[2] Zhu J G J and Park C 2006 *Mater. Today* **9** 36
[3] Hirohata A, Yamada K, Nakatani Y, Prejbeanu I L, Diény B, Pirro P, and Hillebrands B 2020 *J. Magn. Magn. Mater.* **509** 166711
[4] He B, Hu Y, Zhao C, Wei J, Zhang J, Zhang Y, Cheng C, Li J, Nie Z, Luo Y, Zhou Y, Zhang S, Zeng Z, Peng Y, Coey J M D, Han X, and Yu G 2023 *Adv. Electron. Mater.* **9** 2201240
[5] Miao G X, Münzenberg M, and Moodera J S 2011 *Rep. Prog. Phys.* **74** 036501
[6] Botsch L, Lorite I, Kumar Y, Esquinazi P D, Zajadacz J, and Zimmer K 2019 *ACS Appl. Electron. Mater.* **1** 1832
[7] Novoselov K S, Mishchenko A, Carvalho A, and Neto A H C 2016 *Science* **353** aac9439
[8] Liu Y, Huang Y, and Duan X 2019 *Nature* **567** 323
[9] Liang S J, Cheng B, Cui X, and Miao F 2019 *Adv. Mater.* **32** 1903800
[10] Castellanos-Gomez A, Duan X, Fei Z, Gutierrez H R, Huang Y, Huang X, Quereda J, Qian Q, Sutter E, and Sutter P 2022 *Nat. Rev. Methods Primers* **2** 58
[11] Zhang Y, Xu H, Feng J, Wu H, Yu G, and Han X 2021 *Chin. Phys. B* **30** 118504
[12] Zhang L S, Zhou J, Li H, Shen L, and Feng Y P 2021 *Phys. Rev. Appl.* **8** 021308
[13] Elahi E, Dastgeer G, Sharma P R, Nisar S, Suleman M, Iqbal M W, Imran M, Aslam M, and Imran A 2022 *J. Phys. D: Appl. Phys.* **55** 423001

[14] Hao Q, Dai H, Cai M, Chen X, Xing Y, Chen H, Zhai T, Wang X, and Han J B 2022 *Adv. Electron. Mater.* **8** 2200164
[15] Deng Y, Yu Y, Song Y, Zhang J, Wang N Z, Sun Z, Yi Y, Wu Y Z, Wu S, Zhu J, Wang J, Chen X H, and Zhang Y 2018 *Nature* **563** 94
[16] Zhang G, Guo F, Wu H, Wen X, Yang L, Jin W, Zhang W, and Chang H 2022 *Nat. Commun.* **13** 5067
[17] Gong C, Li L, Li Z, Ji H, Stern A, Xia Y, Cao T, Bao W, Wang C, Wang Y, Qiu Z Q, Cava R J, Louie S G, Xia J, and Zhang X 2017 *Nature* **546** 265
[18] Wang Y P and Long M Q 2020 *Phys. Rev. B* **101** 024411
[19] Wimmer S, Sánchez-Barriga J, Küppers P *et al.* 2021 *Adv. Mater.* **33** 2102935
[20] Wang Z, Gibertini M, Dumcenco D, Taniguchi T, Watanabe K, Giannini E, and Morpurgo A F 2019 *Nat. Nanotechnol.* **14** 1116
[21] Otrokov M M, Klimovskikh I I, Bentmann H *et al.* 2019 *Nature* **576** 416
[22] May A F, Calder S, Cantoni C, Cao H, and McGuire M A 2016 *Phys. Rev. B* **93** 014411
[23] Niu W, Cao Z, Wang Y, Wu Z, Zhang X, Han W, Wei L, Wang L, Xu Y, Zou Y, He L, and Pu Y 2021 *Phys. Rev. B* **104** 125429
[24] Hu C, Zhang D, Yan F, Li Y, Lv Q, Zhu W, Wei Z, Chang K, and Wang K 2020 *Sci. Bull.* **65** 1072
[25] Hu C, Yan F, Li Y, and Wang K 2021 *Chin. Phys. B* **30** 097505
[26] Zheng Y, Ma X, Yan F, Lin H, Zhu W, Ji Y, Wang R, and Wang K 2022 *npj 2D Mater.* **6** 62
[27] Wang Z, Sapkota D, Taniguchi T, Watanabe K, Mandrus D, and Morpurgo A F 2018 *Nano Lett.* **18** 4303
[28] Min K H, Lee D H, Choi S J, Lee I H, Seo J, Kim D W, Ko K T, Watanabe K, Taniguchi T, Ha D H, Kim C, Shim J H, Eom J, Kim J S, and Jung S 2022 *Nat. Mater.* **21** 1144
[29] Albarakati S, Tan C, Chen Z J, Partridge J G, Zheng G, Farrar L, Mayes E L H, Field M R, Lee C, Wang Y, Xiong Y, Tian M, Xiang F, Hamilton A R, Tretiakov O A, Culcer D, Zhao Y J, and Wang L 2019 *Sci. Adv.* **5** eaaw0409
[30] Lin H, Yan F, Hu C, Lv Q, Zhu W, Wang Z, Wei Z, Chang K, and Wang K 2020 *ACS Appl. Mater. Interfaces* **12** 43921
[31] Zhu W, Lin H, Yan F, Hu C, Wang Z, Zhao L, Deng Y, Kudrynskyi Z R, Zhou T, Kovalyuk Z D, Zheng Y, Patanè A, Žutić I, Li S, Zheng H, and Wang K 2021 *Adv. Mater.* **33** 2104658
[32] Wang Z A, Xue W, Yan F, Zhu W, Liu Y, Zhang X, Wei Z, Chang K, Yuan Z, and Wang K 2023 *Nano Lett.* **23** 710
[33] Carteaux V, Brunet D, Ouvrard G, and Andre G 1995 *J. Phys.: Condens. Matter* **7** 69
[34] Sharma M, Wang S X, and Nickel J H 1999 *Phys. Rev. Lett.* **82** 616
[35] Daqiq R and Ghobadi N 2016 *J. Supercond. Nov. Magn.* **29** 1675
[36] Lin H, Yan F, Hu C, Zheng Y, Sheng Y, Zhu W, Wang Z, Zheng H, and Wang K 2022 *Nanoscale* **14** 2352
[37] Tsymbal E Y, Mryasov O N, and LeClair P R 2003 *J. Phys.: Condens. Matter* **15** R109